



HAL
open science

Dose-dependent strain localization and embrittlement in ferritic materials: a predictive approach based on sub-grain plasticity modelling

Christian Robertson, Li Yang, Bernard Marini

► To cite this version:

Christian Robertson, Li Yang, Bernard Marini. Dose-dependent strain localization and embrittlement in ferritic materials: a predictive approach based on sub-grain plasticity modelling. *Journal of Nuclear Materials*, 2021, 559, pp.153417. 10.1016/j.jnucmat.2021.153417 . cea-03467617

HAL Id: cea-03467617

<https://cea.hal.science/cea-03467617>

Submitted on 6 Dec 2021

HAL is a multi-disciplinary open access archive for the deposit and dissemination of scientific research documents, whether they are published or not. The documents may come from teaching and research institutions in France or abroad, or from public or private research centers.

L'archive ouverte pluridisciplinaire **HAL**, est destinée au dépôt et à la diffusion de documents scientifiques de niveau recherche, publiés ou non, émanant des établissements d'enseignement et de recherche français ou étrangers, des laboratoires publics ou privés.



Distributed under a Creative Commons Attribution - NonCommercial - NoDerivatives 4.0 International License

Dose-dependent strain localization and embrittlement in ferritic materials: a predictive approach based on sub-grain plasticity modelling

C. Robertson¹, Y. Li^{1,2}, B. Marini¹

¹Université Paris-Saclay, CEA, Service de Recherches Métallurgiques Appliquées, 91191, Gif-sur-Yvette, France

²Current address: University of California, Los Angeles, Mechanical and Aerospace Engineering Department, Nano-Micro Mechanics Laboratory, USA

Abstract

This paper presents a theoretical approach addressing plastic-strain spreading in post-irradiated BCC materials accounting for crucial sub-grain scale, dislocation-mediated plasticity mechanisms. The proposed model explicitly provides the number of shear-bands developed in irradiated (N_{irr}) versus non-irradiated (N_{0dpa}) grain cases, for fixed amounts of plastic deformation. Calculations carried out under various irradiation defect size and number density cases, which helps it appraising important material properties, in particular the dose-dependent, grain-scale uniform elongation threshold. The model ability to handle macro-scale effects is then evaluated using a simple stochastic calculation procedure, taking advantage of actual grain size and orientation maps. The dose-dependent embrittlement amplitude appears to critically depend on the shear band thickness and spacing variations, existing near the fracture surface of failing specimens. That perception allows comparing our predictions with adapted test results, for validation.

Keywords: dislocation, shear bands, plastic strain and fracture toughness

1. Introduction

Ferritic (Body Centre Cubic) materials exposed to neutron irradiation develop complex defect microstructures, including mobile and immobile point defects and clusters, of both interstitial and vacancy types. The irradiation defect populations can then interact with dislocation-mediated plasticity mechanisms controlling the material stress-strain response, as evidenced by direct experimental [1-11] or numerical modelling investigations, including molecular dynamics (MD) [12-14] and dislocation dynamics (DD) [15-18]. Dislocation/defect interactions usually thus explain material hardening, loss of ductility and embrittlement, affecting the operational lifetime of neutron-exposed, reactor components [15-19]. Earlier investigation of dose-dependent plasticity mechanisms has shown that:

- 1) sub-grain plastic strain spreading takes the form of regularly spaced, wavy shear bands, allegedly controlling the material stress-strain response, before and after irradiation [20-24];
- 2) the number of shear bands per unit grain surface decreases with the dose, for a given defect size and plastic strain level [25-26]. Strain localisation effect generates high local stress conditions on internal material interfaces (at grain boundaries, for example), thereby degrading the post-irradiation ductility of polycrystalline materials;
- 3) disperse defect population significantly affects the effective dislocation mobility, depending on the irradiation defect size and number densities [27-29];
- 4) mobile dislocations tend to follow a path of least resistance, by way of cross-slip mechanism: this situation significantly lowers the effective defect strength, no matter the defect type involved [30-31].

This paper presents a plastic-strain spreading model based on crucial sub-grain plasticity mechanisms supported by recent DD simulation results [28-29], The present model was first

developed for FCC [32] and then BCC materials [20], for straining temperature $T = 300\text{K}$ and single slip conditions, in consistence with observations of post-irradiated, strained specimens [23,24,33].

The paper is organized as follows. The model constituents (assumptions, expressions, etc.) are explained in Section 2.1, together with a systematic method for generating different, realistic test-cases (in Section 2.2). In Section 3, we explore the typical strain/dose dependent evolutions. In section 3.1 for instance, we analyze the relation existing between plastic-strain spreading and uniform-elongation threshold, in single grains. The calculation results are carried out and analyzed accounting for broad plastic strain evolutions. In Section 3.2, the model ability to capture macro-scale effects is evaluated at selected, fixed plastic strain levels, using a specific stochastic calculation approach, based on microstructural (SEM and EBSD) observations. The main conclusions drawn from the above investigations are summarized in Section 4.

2 Investigation methods

2.1 Dose-dependent plastic strain spreading model

Calculation of the shear band spacing. Our model is developed based on earlier investigation of plasticity mechanisms, using three-dimensional dislocation dynamics simulations: please refer to [20] for details. The work hardening response of bcc-Fe grains can generally be described based on the total dislocation density evolutions, noted ρ_t [21]. These evolutions can be calculated using dislocation multiplication/annihilation balance equations, where ρ_t typically varies as:

$$\rho_t = \rho_0 + \frac{2E}{b} \gamma_p \quad (1)$$

where ρ_0 the initial dislocation density (in m^{-2} units); b the Burgers vector magnitude (in m units) and γ_p the cumulated plastic strain magnitude.

Quantity E expressed in m^{-1} units and is interpreted as the reciprocal mean free path of mobile dislocations, accounting for dislocation/dislocation and dislocation/defect interactions and cross-slip. This variable is temperature-independent in the 100-300K range (and possibly beyond), under controlled strain rate loading conditions. Quantity E is generally dose-dependent and varies as:

$$E(n, D) = \psi \cdot [b \cdot n \cdot D] + E_0 \quad (2)$$

where ψ is a dimensionless coefficient that scales dislocation/defect interaction rate per unit strain (ψ ranges 0.5-1.0 depending on causes affecting the cross-slip rate, like precipitates), n is the defect number density (in m^{-3}), D the defect size (in m) and E_0 the reciprocal mean free path of un-irradiated grains (where $5 \times 10^4 < E_0 < 10^5 \text{ m}^{-1}$ [21]). The applied stress $\Delta\tau_{app}$ accumulated past the reference (un-irradiated) material yield point can then be expressed as:

$$\Delta\tau_{app} = \alpha\mu b\sqrt{\Delta\rho_t} = \alpha\mu b\sqrt{\Delta\rho_0 + \frac{2E(n,D)}{b}\Delta\gamma_p} \quad (3)$$

where α is a dimensionless coefficient fixing the effective interaction strength characterizing dislocation/dislocation and/or dislocation/defect interactions, μ the shear modulus (in MPa); $\Delta\rho_0$ is the (pre-straining) defect number density including the disperse dislocation loop population and $\Delta\gamma_p$ the plastic strain increment considered. Applied stress evolution $\Delta\tau_{app}$ is assumed to be the main cause for dislocation multiplication, in the form of dislocation shear bands. Eq. (3) is used for simplicity and compatibility with [20,32]; and for its ability to capture the dose-dependent evolution of the macroscopic hardening, at least to the first order [21]. Alternate superposition of strengthening expressions have been proposed elsewhere [34,35] and might be used in the future, if necessary.

The back-stress due to a single, isolated pile-up is given by the following analytical expression:

$$\Delta\tau_{app} = \left[\frac{1}{S} \frac{\mu}{(1-\nu)} \right] \Delta\gamma_p \quad (4)$$

where ν is Poisson's coefficient and S a dimensionless parameter characterizing the pile-up (or grain) geometry [36]. A simple, yet more realistic strained-induced dislocation microstructure consist of a set of N parallel, mutually interacting shear bands. In these conditions, the stress due to the j -th shear band standing at a distance X from the i -th shear band depends on a simple decay function:

$$\Delta\tau_{j \rightarrow i} = -\Delta\tau_j \exp\left(-k(z) \frac{|X|}{l}\right) \quad (5)$$

where $k(z)$ is a positive function of coordinate z parallel to the slip plane considered [28,32], X is the distance normal to the (same) slip plane and l a pile-up length characterizing the number of shear loops generated in the i -th shear band. The stress and strain responses of those shear bands is then expressed using a set of N coupled equations (see expressions (8)-(10) of reference [20] for details). Summing-up the N different terms $\Delta\gamma_p = \sum_{i=1}^N \Delta\gamma_i$ and further rearrangement leads to:

$$\Delta\tau_{app} = \frac{\mu}{S(1-\nu)} \left[\frac{1 + \exp\left(-k \frac{\lambda}{D_g}\right)}{2 + (N-2) \left(1 - \exp\left(-k \frac{\lambda}{D_g}\right)\right)} \right] \Delta\gamma_p \quad (6)$$

where D_g is the effective grain size (see Section 2.2); λ is the characteristic inter-band separation and $k = k_{max}(z)$ is a tuning factor for the internal stress, depending on the local dislocation configuration [28]. Namely, parameter $k \approx 5$ applies to FCC materials, holding shear bands including 2D dislocation pile-ups [32]. Parameter $k \approx 1.75$ applies to BCC materials, holding shear bands including diffuse, 3D dislocation stacks [20,28]. Shear bands actually spread out and then broaden up by successive dislocation bursts, as shown in [37]. If the lattice

friction stress is limited¹, stress increment $\Delta\tau_{app}$ from Eq. (3) is then comparable to the shear-band mediated stress increment, from Eq. (6). Inserting $d = D_g/N$ and $\lambda \sim \sqrt{bD_g/\Delta\gamma_p}$ in Eq. (6), i.e. assuming equally spaced shear bands and uniform dislocation density [20,21], we may then write:

$$\frac{\alpha\mu b\sqrt{\Delta\rho_0 + \frac{2E}{b}\Delta\gamma_p}}{\Delta\gamma_p} = \frac{\Delta\tau_{app}}{\Delta\gamma_p} \approx \frac{\mu}{5(1-\nu)} \left[\frac{1 + \exp\left(-k\frac{d}{\sqrt{bD_g/\Delta\gamma_p}}\right)}{2 + (N-2)\left(1 - \exp\left(-k\frac{d}{\sqrt{bD_g/\Delta\gamma_p}}\right)\right)} \right] \quad (7)$$

for simplicity. Eq. (7) allows finding the (dose-dependent) shear band spacing d (or shear band number N) consistent with an effective grain size D_g , plastic strain increment $\Delta\gamma_p$ and dose-dependent work-hardening rate $\Delta\tau_{app}/\Delta\gamma_p$. Eq. (7) also implies that shear band multiplication is mainly controlled by cross-slip mechanism as explained next below [20,32].

Calculation of the shear band thickness. Prior observations reveal that shear bands form at an early deformation stage and then gradually broaden up, with plastic strain accumulation [20,32,37]. The band broadening mechanism is in fact mainly due to dislocations cross-slipping out of adjacent shear bands. Cross-slipped dislocation usually take the form of dislocation sources, generating d -sized pile-ups or 3D stacks (according to Eq. (7)). These dislocation arrangements in turn controls the local (band-scale) stress landscape and therefore, the shear band thickness.

In these conditions, the maximum effective resolved shear stress τ_{eff} acting in a given (primary) shear band sits at (or near) primary/secondary band intersections [32]. This max local stress can be expressed as:

¹ In practice: if the straining takes place at room temperature or beyond.

$$\tau_{eff} = \Delta\tau_{app} + \tau_{int} \quad (8)$$

where τ_{int} is the internal stress that can be represented using a simple decay function, applicable to the secondary dislocation shear bands, namely:

$$\tau_{int} = \Delta\tau_{app} \exp\left(-k \frac{|y|}{l}\right) \quad (9)$$

where y is the normal distance to the primary slip plane and l the characteristic length of the secondary bands or pile-ups. Shear bands span wherever τ_{eff} exceeds the radiation defect strength τ_{defect} corresponding to ~ 2.2 times the critical «Orowan» stress [38], for a given irradiation defect size and spacing [13,37]. Combining Eqs. (8) with (9) and putting $\tau_{eff} = \tau_{defect}$ yields:

$$t_{SB} = -\frac{l}{k} \ln\left(\frac{\Delta\tau_{app} - \tau_{defect}}{\Delta\tau_{app}}\right) \quad (10)$$

where t_{SB} is the shear band thickness and $l = d$ the shear band spacing obtained from Eq. (7). Condition $\Delta\tau_{app} < \tau_{defect}$ is associated with the formation of relatively thick shear bands. Condition $\Delta\tau_{app} > \tau_{defect}$ in contrast corresponds to shear bands of minimal thickness and maximal strain localisation (see also Fig. 3 below) [37].

[Insert table 1 about here]

In brief: our model assumes that the shear spacing and thickness depend, to the first order, on two distinct (though non-independent) internal lengths. Namely the effective grain size controls the (sub-grain scale) inter shear band distance, as per Eq. (7); which in turn controls the (sub-band scale) shear band broadening, as per Eq. (10). The disperse barrier hardening effect is the sole dose-dependent cause considered this far (e.g. Eq. (3)). Additional causes including dislocation source decoration [39,40] may as well contribute to the actual shear band

arrangement and corresponding stress-strain response. These effects are currently under investigation and will be presented separately.

2.2 Stochastic evaluation: grain aggregate and irradiation defect dispersions cases

Plastic strain spreading evolutions can be generated from Eq. (7) using Table 1 input and a fixed grain size. Repeating this evaluation for a large number of realistic grain size cases may help assessing the single-grain→poly-crystal scale transition. In this paper, stochastic evaluation are carried out based on existing grain size and orientation data [31], from Figs. 1a and 1b (for example). In practice, an «effective grain size» D_g^{eff} is assigned to each EBSD data point and calculated as $D_g^{eff} = M_\theta \delta$ where M_θ is the number of consecutive measurements for which the disorientation angle $\theta \leq 5^\circ$ along a given measurement line. In practice, we use parameter $\delta = 0.5 \mu\text{m}$ corresponding to the EBSD scan step size. The same angular threshold (5°) is used in both Figs. 1a and 1b cases, yielding effective grain size distributions of Figs. 1c and 1d consistent with [20,21]. It is believed that D_g^{eff} is a reasonably good approximation of the gliding distance accessible to dislocations sitting at or near the considered measurement point. In the rest of the paper, «grain size» D_g actually refers to D_g^{eff} unless otherwise specified.

[Insert Figure 1 about here]

Stochastic evaluations based on Fig. 1 aggregates are carried out (see Section 3.2) for two distinct irradiation conditions, characterized by 2 distinct disperse defect populations: a high density of small irradiation defects «irradiation 1»; a smaller density of larger irradiation defects «irradiation 2». These conditions (see Table 2) provide a strong irradiation-dependent contrast while avoiding high-dose effects, including solute atom segregations at internal interfaces.

Condition 1 and 2 refer to actual post-irradiation studies of ferritic nuclear materials: 2 dpa at 300°C and 12 dpa at 360°C, as reported in [41] and [42], respectively.

[Insert Table 2 about here]

3 Results

3.1 Plastic strain spreading: assessment of dose-dependent evolutions

In this section, typical Eqs. (1)-(10) evolutions are calculated using Table 1 input values. The dimensionless interaction strength coefficient $\alpha = 0.4$ (see Eq. (3)) applies to various dislocation/loop interaction cases, in various metallic alloys [18]. Quantity $\Delta\tau_{app}$ is the stress amount cumulated past the yield point calculated according to Eq. (3), depending on the irradiation case selected. We take $\tau_{app} = \tau_{YS} + \Delta\tau_{app}$ where $\tau_{YS} \approx 200$ MPa corresponds to the reference material yield stress, before irradiation [43].

The dose-dependent $N(\Delta\gamma_p)$ evolutions are carried out first, by solving Eq. (7) for N under various $E(n, D)$ cases (e.g. Eq. (2)) and using 2 fixed grain sizes D_g . The reference (un-irradiated) $N(\Delta\gamma_p)$ evolution is obtained next, by solving Eq. (7) again; this time using $E(00dpa)$ instead of $E(n, D)$. Plastic strain spreading associated with a particular (n, D) condition is characterized by a strain spreading ratio N_{irr}/N_{00dpa} , where $N_{irr}/N_{00dpa} < 1$ denotes radiation-induced, plastic strain localisation. In any case, we found that N_{irr}/N_{00dpa} gradually increases with the plastic strain $\Delta\gamma_p$ and defect number density n (or dose level), whereas N_{irr}/N_{00dpa} decreases with grain size D_g (see Fig. 2).

[Insert Figure 2 about here]

During actual tensile tests, strain spreading ratio N_{irr}/N_{00dpa} gradually increases up to $N_{irr,crit}/N_{00,crit}$ at $\Delta\gamma_p = UE_{MAX}$, the maximal uniform elongation level achieved at the grain scale, for a given (n, D) irradiation case (see also Section 3.2.2). Quantity $N_{irr,crit}$ is calculated first, by solving Eq. (7) for N assuming $d \rightarrow 0$ (high-strain limit case), using $\tau_{app} = \tau_{YS} + \Delta\tau_{app} \approx \tau_{crit}$ and plastic strain level $\Delta\gamma_p = \Delta\gamma_{p,crit}$. The critical plastic strain level can be evaluated by solving Eq. (3) for $\Delta\gamma_p$, taking² $\Delta\tau_{app} \approx (\tau_{crit} - \tau_{YS}) = (350 - 200)$ MPa and different (n, D) combinations.

Strain level $\Delta\gamma_{p,crit} \sim 2.2 \times 10^{-2}$ is obtained using $n = 1.8 \times 10^{23} \text{ m}^{-3}$ and $D = 2.5 \text{ nm}$, for example. We then find $N_{00,crit}$ in un-irradiated case by solving (modified) Eq. (7) for N again, this time using $E(00dpa)$ instead of $E(n, D)$. Strain spreading ratio $N_{irr,crit}/N_{00,crit}$ results are shown in Fig. 3a, for 2 different defect sizes and defect number density evolutions up to $2 \times 10^{24} \text{ m}^{-3}$. Plastic strain ratio $N_{irr,crit}/N_{00,crit}$ gradually decreases within a certain dose range, i.e. up to a critical irradiation defect number density (or dose), for a fixed irradiation defect size. The maximum dose correspond to $\tau_{internal} \geq \tau_{defect}$, where mobile dislocations cut through the whole irradiation defect population and glide unhindered, up to the grain boundaries [37]. In this situation, shear band thickness $t_{SB} \rightarrow 0$ and grains (or grain boundaries) may fail following very little (or no) plastic strain accumulation [37]. And hence, the dose-range compatible with $UE_{MAX} > 0$ may critically depends on the shear band thickness t_{SB} evolutions as shown in Fig. 3b, for different defect sizes and number densities up to $2 \times 10^{24} \text{ m}^{-3}$. Fig. 3a results are fully consistent with reference [22], if the (macroscopic) uniform elongation evolutions precisely

² Fig. 12 of reference [9] indicates $\tau_{crit} \approx 350$ MPa, in typical ferritic steels.

scales with those of its grain-scale counterpart: $\Delta\gamma_{p,crit}(n, D)$. This comparison is consistent with (poly-crystalline) specimen failure due to an avalanche-like mechanism, triggered as soon as condition $\Delta\gamma_{p,crit}$ is satisfied in (at least) a fraction of the grains.

[Insert Figure 3 about here]

3.2 Dose-dependent plastic strain spreading in grain aggregates: a stochastic evaluation

3.2.1 Sub-grain shear band spreading

In this section, section 3.1 model ability to address macroscopic-scale effects is evaluated using a simple stochastic calculation procedure, taking advantage of available grain aggregate data sets. The evaluation is carried out in terms of shear band spacing and thickness, by solving Eq. (3) using the local effective grain size assigned to each EBSD data point (see Section 2.2). Fig. 4 results are obtained assuming critical applied stress level $\tau_{app} \approx \tau_{crit}$ i.e. under loading/straining conditions fairly representative of fracture-related, plasticity mechanisms (see Section 3.1). In practice, the present calculations also assume that:

- 1) the applied stress level is uniform (though the internal stress is not), everywhere in the grain aggregate (see Section 2.2);
- 2) the cumulated plastic strain level is uniform, everywhere in the grain aggregate;
- 3) plastic strain develops under single slip conditions; in consistence with direct observations of post-irradiated materials [1-10],
- 4) the mutual, grain to grain mutual interactions are negligible, which implies that grains of same size, geometry and orientations have the same (sub-grain) shear band distributions, regardless of the neighbouring grain environment.

The shear band thickness and spacing results (see Fig. 4) hence vary from one EBSD measurement point to another, in order to satisfy the above 1-3 conditions, everywhere in the investigated poly-crystal. Shear band spacing distribution obtained in irradiation conditions 1 and 2 are mostly identical, for a given material microstructure (compare cases 1 and 3; then cases 2 and 4, in Fig. 4). Fig. 4b and 4d results scale with the barrier hardening amplitude, since the nD product is practically the same, in condition 1 and condition 2. The shear band thickness distribution in irradiation condition 2 is significantly broader than irradiation condition 1, however (compare Fig. 4a to 4c). Shear band thickness is $\propto 1/D$ and therefore directly depends on the local stress landscape, at the scale of individual irradiation defect clusters [28].

Fig. 4 results highlight the effect of grain size and geometry variations, in the considered grain aggregates. It is in principle possible to validate Fig. 4 results by comparison with direct observation of the surface slip markings of a strained specimens. An alternative (cost and time effective) comparison method is possible yet, by supposing that shear band thickness and spacing have direct consequences on the poly-crystal failure response. Section 3.2.2 represents an indirect evaluation attempt based on suitable tests results and recent progress on plasticity mechanisms modelling [28,29].

[Insert Figure 4 about here]

3.2.2 Effect plastic strain spreading on the dose-dependent material fracture response

- I) Plastic strain spreading and upper shelve energy evolutions

Irradiation embrittlement generally produce an upward shift of the ductile to brittle transition temperature and a downward shift of the Upper Shelve Energy (noted USE : see also Fig. 7b), characterizing the material ductile straining regime. We have seen earlier that the N_{irr}/N_{00dpa} ratio gradually increases up to $N_{irr,crit}/N_{00,crit}$ as $\Delta\gamma_p$ increases up to $\Delta\gamma_p = UE_{MAX}$, in irradiated condition (n, D) (see Section 3.1). In this section, we further assume that the USE scales with shear-band emission: greater shear-band emission produces stronger material resistance, against brittle fracture development [44]. In that case, quantity N_{irr} associated with condition (n, D) would naturally scale with Upper Shelve Energy USE associated with the same (n, D) case.

Significant differences are readily observed between the 2 examined aggregate cases in fixed, sub-critical irradiation conditions (compare Fig. 5a and 5b). In irradiation condition 1, minimal $N_{irr}/N_{00dpa} = 0.85$ in case 1 (fine-grained microstructure) and minimal $N_{irr,crit}/N_{00,crit} = 0.9$ in case 2 (coarse-grained microstructure). Those $N_{irr,crit}/N_{00,crit}$ values are consistent with the USE_{irr}/USE_{00dpa} values obtained in post-irradiated FeC alloys holding exactly the same (n, D) defect population as in condition 1 [41,43,45]. In irradiation condition 2, minimal $N_{irr,crit}/N_{00,crit} = 0.80$ is obtained in fine grain microstructure (case 3) and minimal $N_{irr,crit}/N_{00,crit} = 0.85$ in coarse-grained microstructure (case 4). Case 4 values are consistent with USE_{irr}/USE_{00dpa} values observed in irradiated Fe9Cr alloy, in exactly the same (n, D) «condition 2» case [46,47]. The theoretical USE change is therefore smaller in irradiation condition 2 than in irradiation condition 1, regardless of the material microstructure.

[Insert figure 5 about here]

II) Dislocation mobility, embrittlement and transition temperature shift evolutions.

This sub-section addresses the relation existing between plastic strain spreading and material embrittlement. More specifically, correlations are drawn between Section 3.2.1 calculations and the ductile to brittle transition temperature shift from comparable resilience test results. Dislocation/defect interactions generate multiple pinning points, in the mobile dislocation lines [48]. In controlled strain-rate loading conditions, dislocation/defect interactions specifically affect:

- i- The «defect-free» span of the mobile dislocation lines, $L_0 \rightarrow L_1$ (subscript «0»: un-irradiated material condition; subscript «1»: irradiated material condition);
- ii- the effective stress acting on the mobile dislocations: $\tau_0 \rightarrow \tau_1$;
- iii- the velocity of mobile dislocations: $v_0 \rightarrow v_1$; since $\tau_0 \rightarrow \tau_1$ evolution generally affects dislocation velocity through the kink-pair nucleation rate³, even in absence of any $L_0 \rightarrow L_1$ evolution.

Overall, dislocation/defect interactions yield significant dislocation mobility reduction, depending on the local dislocation/defect configurations and the average, effective defect strength [27,30]. Straining temperature changes likewise affect the dislocation mobility; so it is in principle possible to find a straining temperature (down) shift yielding exactly the same dislocation mobility changes as a given defect population does. It can be shown that those defect-induced changes are correctly captured by a Defect-Induced Apparent straining Temperature shift, noted $\Delta DIAT$ [27-29], that can be calculated using the following, semi-analytical expression:

³ See Eq. (4) in reference [23].

$$\Delta DIAT = \Delta T_{max} \left(1 - \exp\left(\frac{D}{\xi}\right) \right) (1 - \exp(-t_{SB}^2 D n)) \quad (11)$$

Eq. (11) includes three material-dependent parameters, namely: a reference *DIAT* shift ΔT_{max} and characteristic distances ξ and t_{SB} (see more details below). Reference shift value ΔT_{max} is associated with maximal stress change $\tau_0 \rightarrow \tau_{1,MAX}$ and corresponding dislocation velocity evolution $v_0 \rightarrow v_{1,MAX}$. Such (extremal) stress/velocity evolution is concurrent with: i) strictly coplanar dislocation/defect interactions, ii) hard, non-shearable defects, iii) saturation defect number density $n = n_{sat}$. Reference shift $\Delta T_{max} \sim 200\text{K}$ is obtained in irradiation case 1 and $\Delta T_{max} \sim 230\text{K}$ in irradiation case 2, assuming defect sizes $D = 1.6 \text{ nm}$ and $D = 2.5 \text{ nm}$ (respectively) and using $n_{sat} = 2 \times 10^{24} \text{ m}^{-3}$, in both cases [47]. Distance t_{SB} can be calculated using Eq. (10) and characterizes the thickness of the shear band contributing to the material fracture response. Parameter $\xi \approx \sqrt{2}(D/D_0)(D^2/t_{SB})$ where $D_0 \approx 2 \text{ nm}$; characterizes the defect-scale stress landscape, within the sub-grain shear bands [27,28].

[Insert Figure 6 about here]

It is important to note that Eq. (11) also works/applies in presence of a heterogeneous crack stress field and therefore, correctly captures the relevant (grain-scale), fracture-related plasticity mechanisms [27]. It is also essential to note that the $\Delta DIAT$ level associated with a fixed reference temperature and defect dispersion (n, D) closely follows the actual $\Delta DBTT$ magnitude achieved in resilience specimens holding a comparable (n, D) defect population [29]. This means the (dose-dependent) ductile to brittle transition temperature shift critically depends on the statistical variations of quantities ξ and t_{SB} , characterizing the internal stress landscape in the highly deformed grains, sitting near the specimen fracture surface.

Eq. (11) formally allows evaluating the nearby material capacity to retard brittle fracture initiation and propagation, thanks to plastic strain spreading. A given $\Delta DIAT$ level is associated with a critical, dose-dependent plastic strain condition. The latter is regarded as a necessary conditions for (post-irradiation) brittle fracture initiation, no matter the fracture initiator type involved [49-53]. This situation implies that the stress acting on brittle fracture initiators sharply augment and the surrounding material quickly fails, as soon as the local stress relaxation capacity is exhausted. Comparison with selected resilience test results is presented next, in an attempt to validate/explore that perception.

The influence of dislocation-mediated plasticity on the $\Delta DIAT$ evolutions is shown in Fig. 6a and 6b, for two different grain sizes D_g and irradiation defect sizes D . The $\Delta DIAT$ distributions corresponding to cases 1-4 are obtained by inserting the shear band thickness data from Fig. 4 (see Figs. 6c and 6d). Case 1 (fine-grained microstructure) yield a mono-modal $\Delta DIAT$ distribution, where the highest probability of occurrence corresponds to $\Delta DIAT = 55^\circ\text{K}$ (see Fig. 6c). Case 2 (coarser grained microstructure) yield a mono-modal $\Delta DIAT$ distribution as well, where $\Delta DIAT = 50^\circ\text{K}$ bears the highest probability of occurrence (see Fig. 6d). $\Delta DIAT$ results shown in Fig. 6c are consistent with the $\Delta DBTT$ results presented in [43], for material microstructures comparable to case 1 and case 2 conditions.

Case 3 (fine-grained microstructure) yields a mono-modal $\Delta DIAT$ distribution, where $\Delta DIAT = 50\text{K}$ holds the highest probability of occurrence. Case 4 (coarser grained microstructure) yield a bimodal $\Delta DIAT$ distribution, where $\Delta DIAT = 40^\circ\text{K}$ and $\Delta DIAT = 120^\circ\text{K}$ have the highest probability of occurrence. Temperature shift $\Delta DIAT = 120^\circ\text{K}$ is consistent with $\Delta DBTT$ measured in grain and irradiation defect microstructures comparable to case 4 conditions; i.e. for Fe9Cr steel irradiated up to 1-2 dpa at $T = 300^\circ\text{C}$ [46]. Fine grained Fe9Cr aggregates (case

3) have a significantly better resistance to irradiation-induced embrittlement than their coarse grained counterpart (case 4).

3.2.3 Brief discussion

Fig. 6 results are consistent with the plasticity mechanisms sketched in Fig. 7a, depending on the irradiation cases. Irradiation condition 1 retains a significant amount of residual ductility, characterized by frequent nucleation of relatively broad (thick) shear bands, near the fracture surface. Shear band structures characterizing irradiation condition 1 implies a fast defect absorption rate (with cumulated plastic strain) and hence, a relatively important remaining dislocation mobility.

Residual (post-irradiation) ductility is much smaller under irradiation condition 2, where the larger defects inhibit shear band multiplication and broadening, leading to thinner shear bands. Dislocation mobility thereof is comparatively lower due to the strong, persistent dislocation trapping effect due to the larger irradiation defects. These defect-dependent changes of plasticity mechanisms are consistent with the resilience curves evolutions pointed out in Fig. 7b.

To conclude this Section, the reader should take note that $\Delta DIAT \sim \Delta DBTT$ condition applies to irradiation cases where dose-dependent segregations and grain size evolutions are limited. Segregations may produce a distinct, non-hardening embrittlement contribution, affecting the actual transition temperature shift magnitude. In its current form, Eq. (11) best applies to ferritic steels for irradiation doses up to 2-3 dpa, at irradiation temperatures up to 400°C [27,28]. Accounting for non-hardening embrittlement causes entails further, ongoing investigation effort.

[Insert Figure 7 about here]

4. Conclusion/summary

This paper presents a model addressing plastic strain spreading in ferritic grains, accounting for irradiation defect populations and crucial, sub-grain plasticity mechanisms. The proposed method provides the explicit number of shear-bands formed in irradiated (N_{irr}) versus non-irradiated (N_{00dpa}) grain cases, for fixed amounts of plastic deformation. The calculations show that:

- 1) the N_{irr}/N_{00dpa} ratio gradually increases with the plastic strain level $\Delta\gamma_p$; whereas $N_{irr}/N_{00dpa} < 1$ denotes plastic strain localisation;
- 2) the N_{irr}/N_{00dpa} ratio sharply decreases with increasing defect size D , for any fixed defect number density n and plastic strain level $\Delta\gamma_p$;
- 3) the shear band spacing distribution essentially depends on the $n \cdot D$ product, thus directly scales with the disperse barrier hardening amplitude;
- 4) the shear band thickness distribution varies as $1/D$ according to the (local) stress landscape;
- 5) the uniform elongation limit at the grain scale depend on the homogeneous ($N_{irr}/N_{00dpa} \geq 1$) to localized ($N_{irr}/N_{00dpa} < 1$) plastic strain spreading transition, itself depending on: i- mutual, shear-band/shear-band interaction strength through parameter $k = k_{max}(z)$; ii- stress limit $\Delta\tau_{app} \approx \tau_{crit}$ relative to the average irradiation defect strength τ_{defect} .

The model ability to address macro-scale effects is evaluated using a simple stochastic calculation procedure; taking advantage of existing grain aggregate data sets. It is recognized

that irradiation-induced embrittlement critically depends on the statistical, shear band thickness and spacing variations, near the fracture surfaces of failing (resilience) specimens. That perception helps it comparing our calculations with available/adapted test results, for partial validation. And hence:

6) theoretical $N_{irr,crit}/N_{00,crit}$ evolutions precisely scale with the experimental USE_{irr}/USE_{00dpa} values, in a given (n, D) condition;

7) the statistical shear-band thickness and spacing variations correspond to $\Delta DIAT$ distributions consistent with the $\Delta DBTT$ changes observed in corresponding resilience specimens, in a given (n, D) condition;

8) the dose-dependent transition-temperature (up)shift markedly depends on the grain size distribution: fine grained aggregates exhibit a better resistance to radiation embrittlement than coarser grained aggregates (i.e. significantly smaller $\Delta DIAT$ amplitudes).

5. Acknowledgment

This work has received funding from the Euratom research and training programme 2014-2018 under grant agreement No. 755039 (M4F project).

6. References

- [1] M. Victoria, N. Baluc, C. Bailat, Y. Dai, M. Lупpo, R. Schaüblin, B. Singh, The microstructure and associated tensile properties of irradiated FCC and BCC metals, J. Nucl. Mater. 276 (2000) 114-122.
- [2] N. Hashimoto, T. Byun, K. Farrell, S. Zinkle, Deformation microstructure of neutron-irradiated pure polycrystalline metals, J. Nucl. Mater. 329 (2004) 947-952.

- [3] N. Hashimoto, T. Byun, K. Farrell, Microstructural analysis of deformation in neutron irradiated FCC materials, *J. Nucl. Mater.* 351 (2006) 295-302.
- [4] Z. Yao, R. Schäublin, M. Victoria, Tensile properties of irradiated Cu single crystals and their temperature dependence, *J. Nucl. Mater.* 329 (2004) 1127-1132.
- [5] T. Byun, K. Farrell, Plastic instability in polycrystalline metals after low temperature irradiation, *Acta Mater* 52 (2004) 1597-1608.
- [6] T. Byun, N. Hashimoto, K. Farrell, Temperature dependence of strain hardening and plastic instability behaviours in austenitic stainless steels, *Acta Mater.* 52 (2004), 3889-3899.
- [7] T. Byun, N. Hashimoto, K. Farrell, Deformation mode map of irradiated 316 stainless steel in true stress-dose space, *J. Nucl. Mater.* 351 (2006) 303-315.
- [8] T. Byun, N. Hashimoto, K. Farrell, E. Lee, Characteristics of microscopic strain localization in irradiated 316 stainless steels and pure vanadium, *J. Nucl. Mater.* 349 (2006) 251-264
- [9] T. Byun, N. Hashimoto, Strain localization in irradiated materials, *Nucl. Eng. and Tech.* 38 (2006) 619-638
- [10] S.J. Zinkle, B.N. Singh, Microstructure of neutron-irradiated iron before and after tensile deformation, *J. Nucl. Mater.* 351 (2006) 269-284
- [11] M. McMurtrey, G. Was, B. Cui, I. Robertson, L. Smith, D. Farkas, Strain localization at dislocation channel-grain boundary intersections in irradiated stainless steel, *Int. J. Plast.* 56 (2014) 219-231.
- [12] D. Terentyev, P. Grammatikopoulos, D. Bacon, Y.N. Osetsky, Simulation of the interaction between an edge dislocation and a $\langle 100 \rangle$ interstitial dislocation loop in α -iron, *Acta Mater* 56 (2008) 5034-5046.
- [13] D. Terentyev, D.J. Bacon, Y.N. Osetsky, Reactions between a $1/2\langle 111 \rangle$ screw dislocation and $\langle 100 \rangle$ interstitial dislocation loops in alpha-iron modelled at atomic scale. *Phil. Mag.* 90 (2010) 1019-1033.

- [14] J. Marian, B.D. Wirth, R. Schäublin, G. Odette, J.M. Perlado, MD modelling of defects in Fe and their interactions, *J Nucl Mater* 323 (2003) 181-191
- [15] J. Marian, G. Po, Discrete dislocation dynamics simulations of irradiation hardening in nuclear materials, DOI: 10.1007/978-3-319-50257-1_121-1 (2018).
- [16] J. Marian, E. Martinez, H.J. Lee, B.D. Wirth, Micro/meso-scale computational study of dislocation-stacking-fault tetrahedron interactions in copper, *J Mater Res* 24 (2009) 3628-3635.
- [17] E. Martinez, J. Marian, A. Arsenlis, M. Victoria, J. Perlado, Atomistically informed dislocation dynamics in FCC crystals, *J Mech. Phys. Solids* 56 (2008) 869-895.
- [18] X. Shi, L. Dupuy, B. Devincere, D. Terentyev, L. Vincent, Interaction of $\langle 1\ 0\ 0 \rangle$ dislocation loops with dislocations studied by dislocation dynamics in α -iron. *J Nucl Mater* 460 (2015) 37-43
- [19] D. Terentyev, G. Monnet, P. Grigorev, Transfer of molecular dynamics data to dislocation dynamics to assess dislocation–dislocation loop interaction in iron, *Scr. Mater.* 69 (2013) 578-581.
- [20] K. Gururaj, C. Robertson, M. Fivel, Post-irradiation plastic deformation in bcc Fe grains investigated by means of 3D dislocation dynamics simulations, *J. Nucl. Mater.* 459 (2015) 194-204.
- [21] K. Obrtlik, C.F. Robertson, B. Marini, Dislocation structures in 16MND5 pressure vessel steel strained in uniaxial tension, *J. Nucl. Mater.* 342 (2005) 35-41.
- [22] K. Farrell, T.S. Byun, N. Hashimoto, Deformation mode maps for tensile deformation of neutron-irradiated structural alloys, *J. Nucl. Mater.* 335 (2004) 471-486.
- [23] D.S. Gelles, R.E. Schäublin, Post-irradiation deformation in a Fe-9%Cr alloy, *Mat. Sci. Eng. A* 309-310 (2001) 82-86.
- [24] M. Eldrup, B.N. Singh, S.J. Zinkle, T.S. Byun, K. Farrell, Dose dependence of defect accumulation in neutron irradiated copper and iron, *J. Nucl. Mater.* 307-311 (2002) 912-917.

- [25] G. Was, J. Busby, Z. Jiao, The Use of Proton Irradiation to Determine IASCC Mechanisms in Light Water Reactors - Phase 3: Deformation Studies. EPRI, Palo Alto, CA: (2006) 1013081.
- [26] B. Sicaud, Multiscale simulations of intergranular fracture initiation in face-centered cubic materials and alloys: influence of the localised plastic slip deformation, Doctoral Thesis, ED 391 SMAER, Paris, (2020).
- [27] Y. Li, C. Robertson, X. Ma, W. Biao, Dislocation spreading and ductile-to-brittle transition in post-irradiated ferritic grains: Investigation of grain size and grain orientation effect by means of 3D dislocation dynamics simulations, *J. Mat. Res.*, 34 (2019) 1584-1594.
- [28] Y. Li, C. Robertson, Irradiation defect dispersions and effective dislocation mobility in strained ferritic grains: A statistical analysis based on 3D dislocation dynamics simulations, *J. Nucl. Mat.* 504 (2018) 84-93.
- [29] Y. Li, C. Robertson, X. Ma, W. Biao, Investigation of Radiation Temperature and Straining Temperature Effects on the Screw Dislocation Mobility Evolution in Irradiated Ferritic Grains Using 3D Dislocation Dynamics, TMS 2019 148th Annual Meeting & Exhib. Supp. Proc. (2019) 1335-1344.
- [30] Y. Li, C. Robertson, M. Shukeir, L. Dupuy, Screw dislocation interaction with irradiation defect-loops in alpha-iron: Evaluation of loop-induced stress field effect using dislocation dynamics simulations, *Nucl. Instr. Meth. in Phys. Res. B*, 458 (2019) 137-142.
- [31] Y. Li, C. Robertson, M. Shukeir, L. Dupuy, Screw dislocation interaction with irradiation defect-loops in alpha-iron: evaluation of cross-slip effect using dislocation dynamics simulations, *Mod. Sim. Mat. Sci. and Eng.*, 26 (2018) 055009.
- [32] K. Gururaj, C. Robertson, M. Fivel, Channel formation and multiplication in irradiated FCC metals: a 3D dislocation dynamics investigation, *Phil. Mag. A*, 95 (2015) 1368-1389.
- [33] L. Malerba et al. Multiscale modelling for fusion and fission materials: the M4F project, *J. Nucl. Energy*, (2021), In press.

- [34] A. de Vaucorbeil, W.J. Poole, C.W. Sinclair, The superposition of strengthening contributions in engineering alloys, *Mater. Sci. and Eng. A* 582 (2013) 147-154.
- [35] M. Lambrecht, E. Meslin, L. Malerba, M. Hernández-Mayoral, F. Bergner, P. Pareige, B. Radiguet, A. Almazouzi, On the correlation between irradiation-induced microstructural features and the hardening of reactor pressure vessel steels, *J. Nucl. Mater.* 406 (2010) 84-89.
- [36] J.P. Hirth, J. Lothe, *Theory of Dislocations*, second ed., Krieger Malabar, Krieger Ln, 1992.
- [37] T. Nogaret, D. Rodney, M. Fivel, C. Robertson, Clear band formation simulated by dislocation dynamics: Role of helical turns and pile-ups, *J. Nucl. Mater.* 380 (2008) 22-29.
- [38] D.J. Bacon, U.F. Kocks, R.O. Scattergood, The effect of dislocation self-interaction on the Orowan stress, *Phil. Mag.* 28 (1973) 1241-1263.
- [39] M.I. Pascuet, E. Martínez, G. Monnet, L. Malerba, Solute effects on edge dislocation pinning in complex alpha-Fe alloys, *J. Nucl. Mater.* 494 (2017) 311-321.
- [40] Zhou, W., Tian, J., Zheng, J. Xue, S. Peng, Dislocation-enhanced experimental-scale vacancy loop formation in hcp Zirconium in one single collision cascade. *Sci Rep.* 6 (2016) 21034. <https://doi.org/10.1038/srep21034>.
- [41] E. Meslin, M. Lambrecht, M. Hernandez-Mayoral, F. Bergner, L. Malerba, A. Almazouzi, Characterization of neutron-irradiated ferritic model alloys and a RPV steel from combined APT, SANS, TEM and PAS analyses, *J. Nucl. Mater.* 406 (2010) 73-83.
- [42] X. Jia, Y Dai, M Victoria, The impact of irradiation temperature on the microstructure of F82H martensitic/ferritic steel irradiated in a proton and neutron mixed spectrum, *J. Nucl. Mat.* 305 (2002) 1-7.
- [43] B. Marini, X. Averty, P. Wident, P. Forget, F. Barcelo, Effect of the bainitic and martensitic microstructures on the hardening and embrittlement under neutron irradiation of a reactor pressure vessel steel, *J. Nucl. Mater.* 465 (2015) 20-27.

- [44] R. Chaouadi, Effect of irradiation-induced plastic flow localization on ductile crack resistance behaviour of a 9%Cr tempered martensitic steel, *J. Nucl. Mater.* 372 (2008) 379-390.
- [45] S.M. Bruemmer, E.P. Simonen, P.M. Scott, P.L. Andresen, G.S. Was, J.L. Nelson, Radiation-induced material changes and susceptibility to inter-granular failure of light-water-reactor core internals, *J. Nucl. Mater.* 274 (1999) 299-314.
- [46] M. Matijasevic, E. Lucon, A. Almazouzi, Behavior of ferritic/martensitic steels after n-irradiation at 200 and 300°C, *J. Nucl. Mater.* 377 (2008) 101-108.
- [47] M. Matijasevic, W. Van Renterghem, A. Almazouzi, Characterization of irradiated single crystals of Fe and Fe-15Cr, *Acta Mater.* 57 (2009) 1577-1585.
- [48] T.D. Swinburne, S.L. Dudarev, Kink-limited Orowan strengthening explains the brittle to ductile transition of irradiated and un-irradiated bcc metals, *Phys. Rev. Mater.* 2 (2018) 073608.
- [49] F.A. Beremin, A local criterion for cleavage fracture of a nuclear pressure vessel steel, *Metall. Trans. A* 14A (1983) 2277-2287.
- [50] P. Bowen, G. Druce, J. F. Knott, Effects of microstructure on cleavage fracture in pressure vessel steel, *Acta metall.* 34 (1986) 1121-1131.
- [51] A.H. Cottrell, Fracture, The Bakerian Lecture 276A (1963) 1-22.
- [52] P. Forget, B. Marini, L. Vincent, Application of local approach to fracture of an RPV steel: effect of the crystal plasticity on the critical carbide size, *Proc. Struct. Integrity* 2 (2016) 1660-1667.
- [53] S. Ren, B. Marini, P. Joly, P. Todeschini, Microstructure-informed modelling of the fracture toughness of alloys representing macro-segregated zones in heavy forgings, *Procedia Structural Integrity* 28 (2020) 684-692.

Table captions

Table 1. List of the main model parameters. The listed values come from various sources: materials handbooks (μ , ν , b , S , τ_{YS}) and open literature data (α , τ_{crit} , E_0 , ψ , k): please refer to the main text.

Table 2. Irradiation conditions selected for the stochastic evaluation of the present plastic strain spreading model (see Section 3.2).

Table 1

μ (GPa)	ν	b (m)	k	S	α	τ_{YS} (MPa)	E_0 (m ⁻¹)	τ_{crit} (MPa)
81	0.3	2.5×10^{-10}	1.75	0.66	0.4	200-250	6.7×10^4	350

Table 2

	Irradiation condition-1 $n = 2 \times 10^{23} \text{ m}^{-3}$ $D = 1.6 \text{ nm}$	Irradiation condition-2 $n = 2 \times 10^{22}$ $D = 10 \text{ nm}$
Microstructure-1: fine grains	Case 1	Case 3
Microstructure-2: coarse grain	Case 2	Case 4

Figure captions

Figure 1. Grain aggregates representative of two distinct model material microstructures, having exactly the same chemical composition. a) Coarser grain microstructure (bainite). b) Finer grain microstructure (martensite). The colours are orientation-specific and highlight the local grain arrangements, whereas the distance indications are in μm units. The effective grain size histograms are evaluated as explained in the main text, for: c) coarse; d) finer grained microstructure cases. All the details regarding the material elaboration and subsequent microstructural analysis are available in reference [31]. The «Relative counts» refers to the effective grain size count over the maximal effective grain size count, in the entire grain aggregate.

Figure 2. Plastic strain ratio evolutions with cumulated plastic strain. The curves clearly show the influence of the irradiation defect number density and grain size, on plastic strain spreading. a) The tested defect number densities are: $n_1 = 1 \times 10^{23} \text{ m}^{-3}$, $n_2 = 1 \times 10^{23} \text{ m}^{-3}$. b) The tested defect number densities are: $n_3 = 3 \times 10^{21} \text{ m}^{-3}$, $n_4 = 3 \times 10^{22} \text{ m}^{-3}$. Comparison between Fig. 2a and 2b show the defect size effect on the plastic strain ratio evolutions. Namely, plastic strain ratio N_{irr}/N_{00dpa} is significantly lower in presence of larger defects, for any fixed irradiation defect number density.

Figure 3. Defect number density effect on the critical shear band spreading variations. a) Critical plastic strain ratio achieved depending on the irradiation defect number density, for irradiation defect sizes 2 and 10 nm. The arrow markers indicate the dose-limit below which UE_{MAX} scales with $N_{irr,crit}/N_{00,crit}$ and beyond which $UE_{MAX} \approx 0$ (see also Fig. 3b hereafter). b) Shear band thickness evolutions with defect number density, for various irradiation defect sizes: 2, 3 and 10 nm. These evolutions are obtained using Eq. (10), where $\Delta\tau_{app}$ comes from Eq. (3); τ_{defect} is 2.2 times the «Orowan» stress and $l = d$ comes from Eq. (7). Shear band thickness t_{SB} vanishes for $n \geq n_{crit}$ (arrow markers), where $UE_{MAX} \approx 0$.

Figure 4. Shear band thickness and spacing distributions in representative grain aggregates. The present stochastic evaluations are carried out using Table 1 material parameters and under critical loading condition $\tau_{app} = \tau_{crit}$ (i.e. UE_{MAX}). Material microstructures 1 and 2 and irradiation conditions 1 and 2 refer to the four cases listed in Table 2. a), b) irradiation condition 1; c), d) irradiation condition 2. The «Relative counts» here refers to the shear band thickness and spacing counts over the maximal shear band thickness and spacing counts obtained, in the considered grain aggregates (see Fig. 1).

Figure 5. Evaluation of plastic strain spreading ratio distributions. The present stochastic calculations are carried out at critical loading level $\Delta\gamma_p = UE_{MAX}$. The material microstructure cases and irradiation conditions refer to Table 2: a) Irradiation condition 1; b) irradiation condition 2. The material microstructure effect (distribution position and width) is better-defined in irradiation Condition 1, i.e. in presence of smaller irradiation defect dispersions. The «Relative counts» refer to the plastic strain spreading ratio counts with respect to the maximal plastic strain spreading ratio count found in the entire grain aggregates (see Fig. 1).

Figure 6. Dislocation mobility indicator $\Delta DIAT$ versus plastic strain spreading evolutions. The calculations are carried out at $\tau_{app} = \tau_{crit}$ using different irradiation defect number densities and sizes: a) $D = 2$ nm; b) $D = 10$ nm. The $\Delta DIAT$ distributions are then evaluated using stochastic procedure as explained in Section 2.2, using material parameters of Table 1. The model material microstructures and irradiation cases refer to Table 2. c) Irradiation condition 1; $\Delta DBTT = 50^\circ\text{C}$ according to [31]. d) irradiation condition 2; $\Delta DBTT = 58^\circ\text{C}$ according to [31]. The $\Delta DIAT$ distribution width reflect the large variety of grain configurations, all over the grain aggregates. The «Relative counts» here refer to the $\Delta DIAT$ counts with respect to the maximal $\Delta DIAT$ count found in the considered grain aggregates (see Fig. 1).

Figure 7. Dose-dependent plastic strain spreading and concurrent fracture-related plasticity mechanism. a) Effect of irradiation defect size and number density on shear band spreading. b) Effect of dislocation-

mediated plasticity mechanisms on the resilience curve. Dose-dependent dislocation mobility changes may explain the transition temperature upshift; dose-dependent plastic strain spreading changes may explain the upper shelf energy downshift.

Figure 1

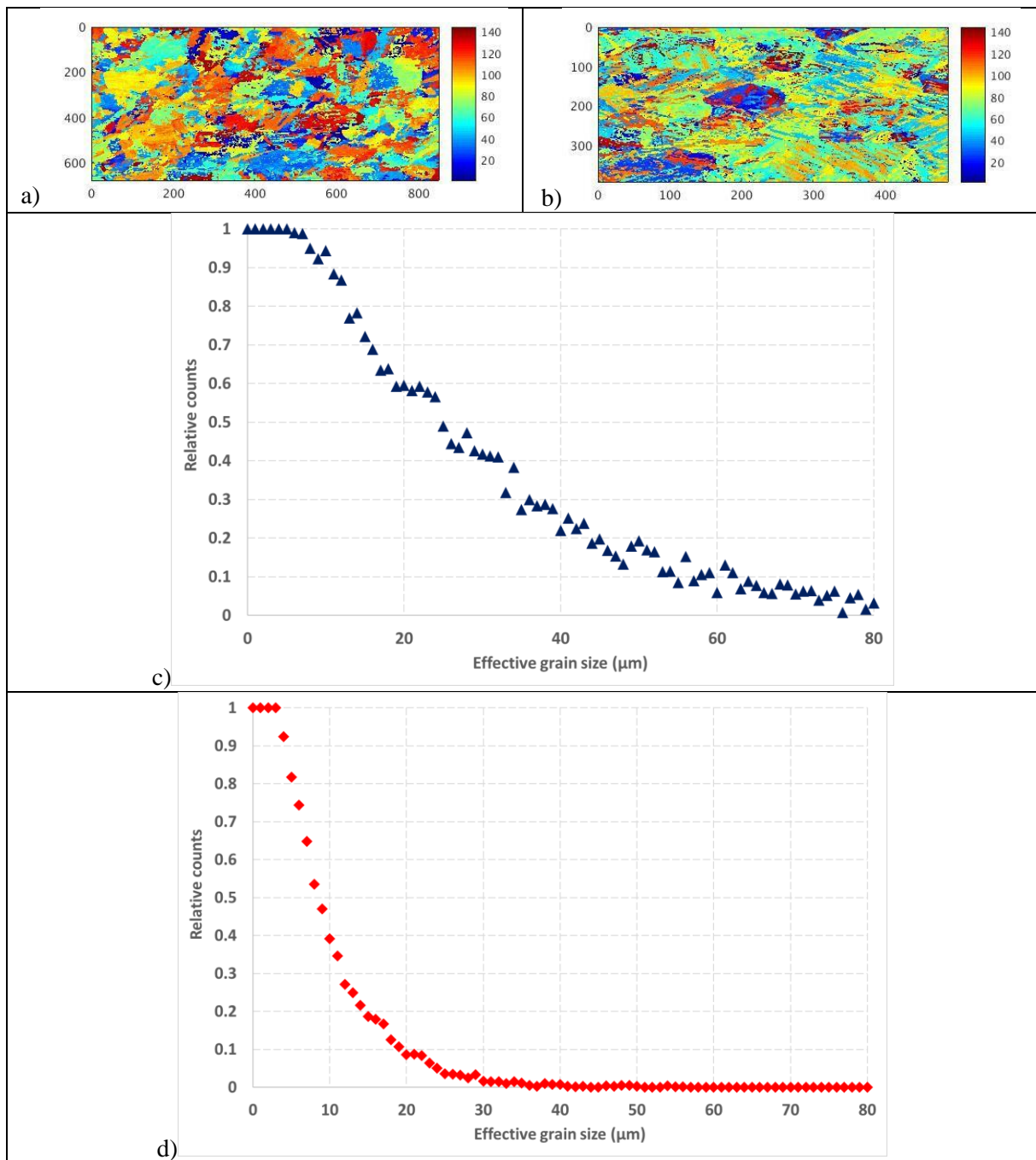


Figure 2

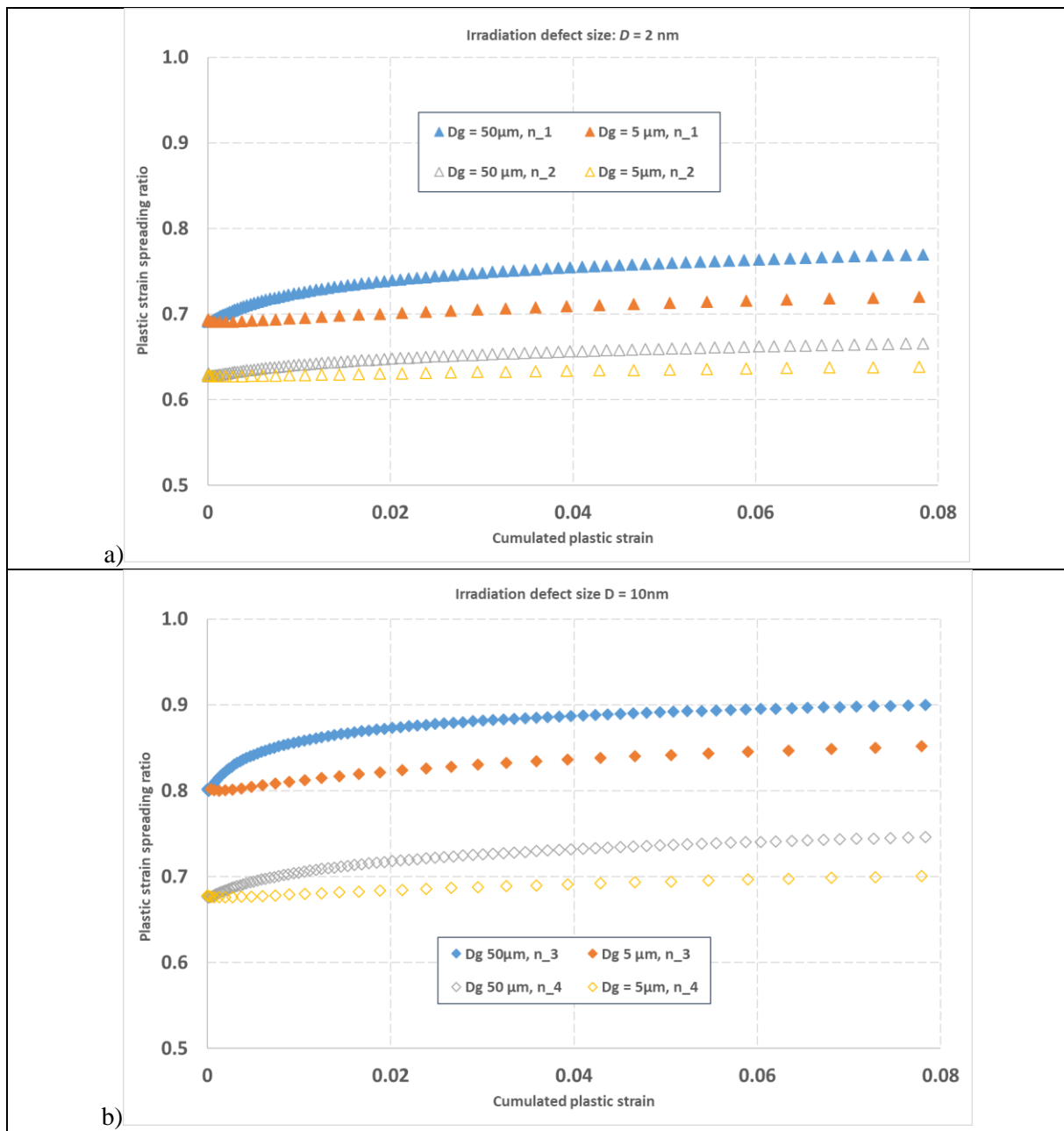


Figure 3

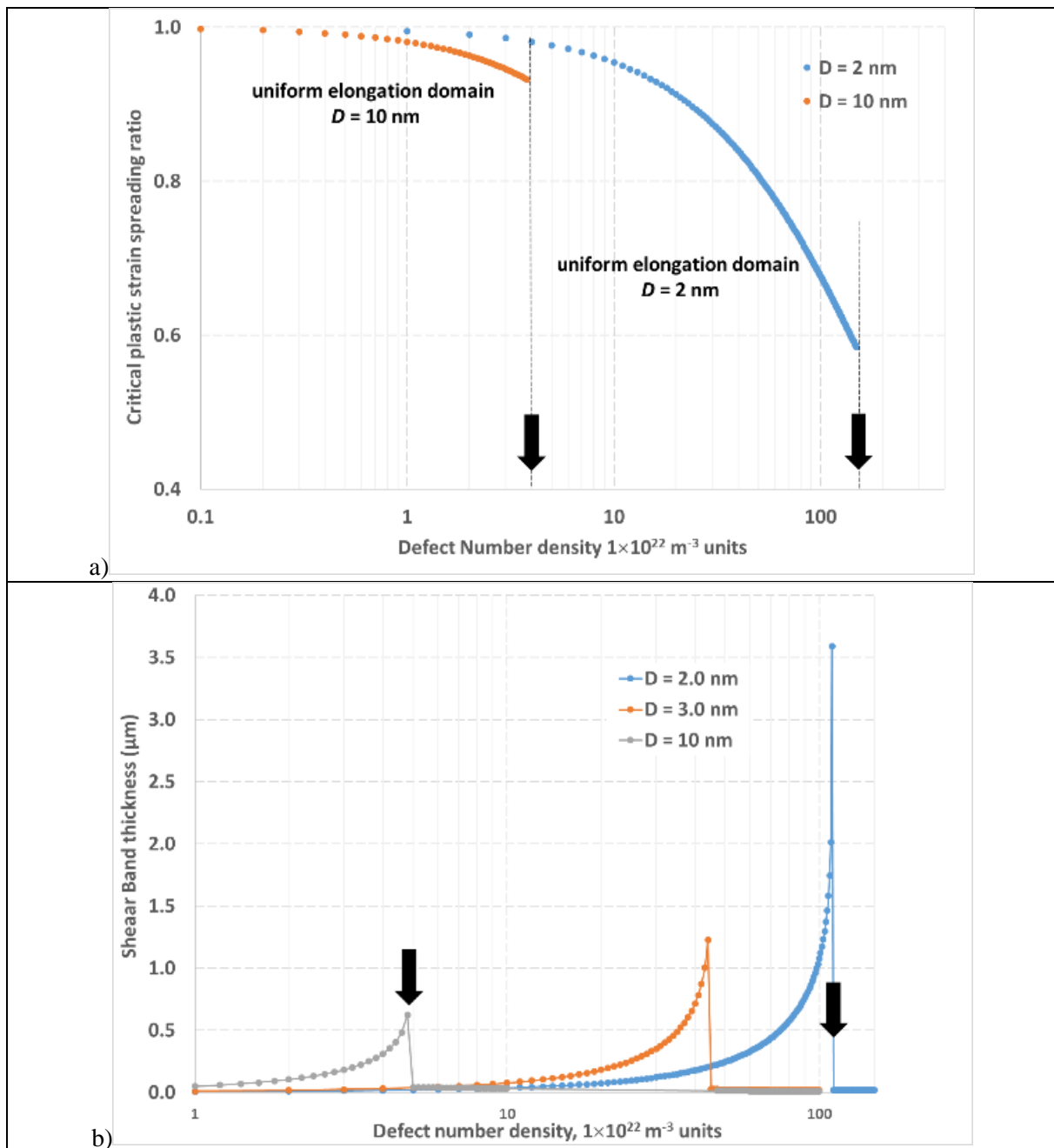


Figure 4

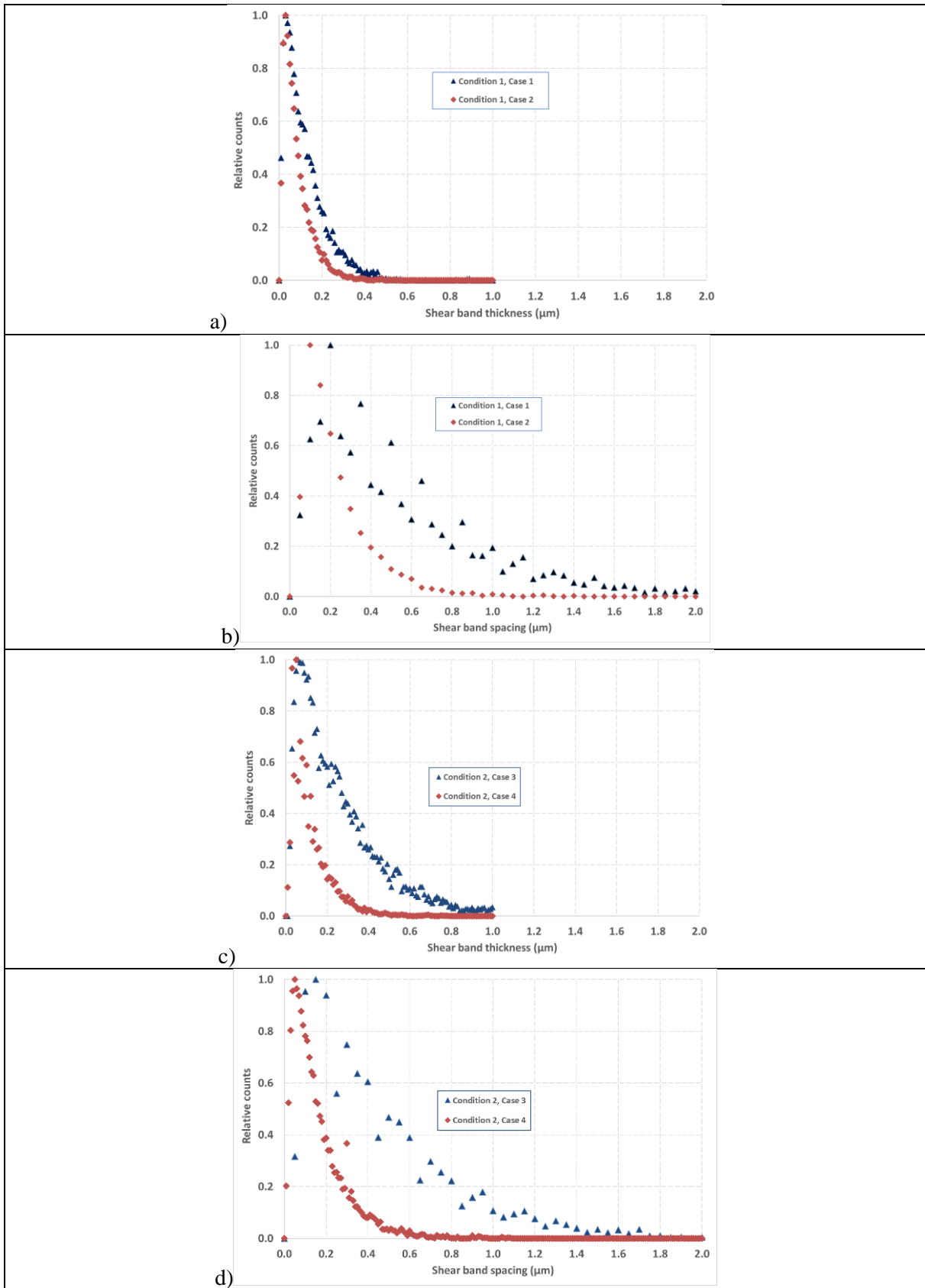


Figure 5

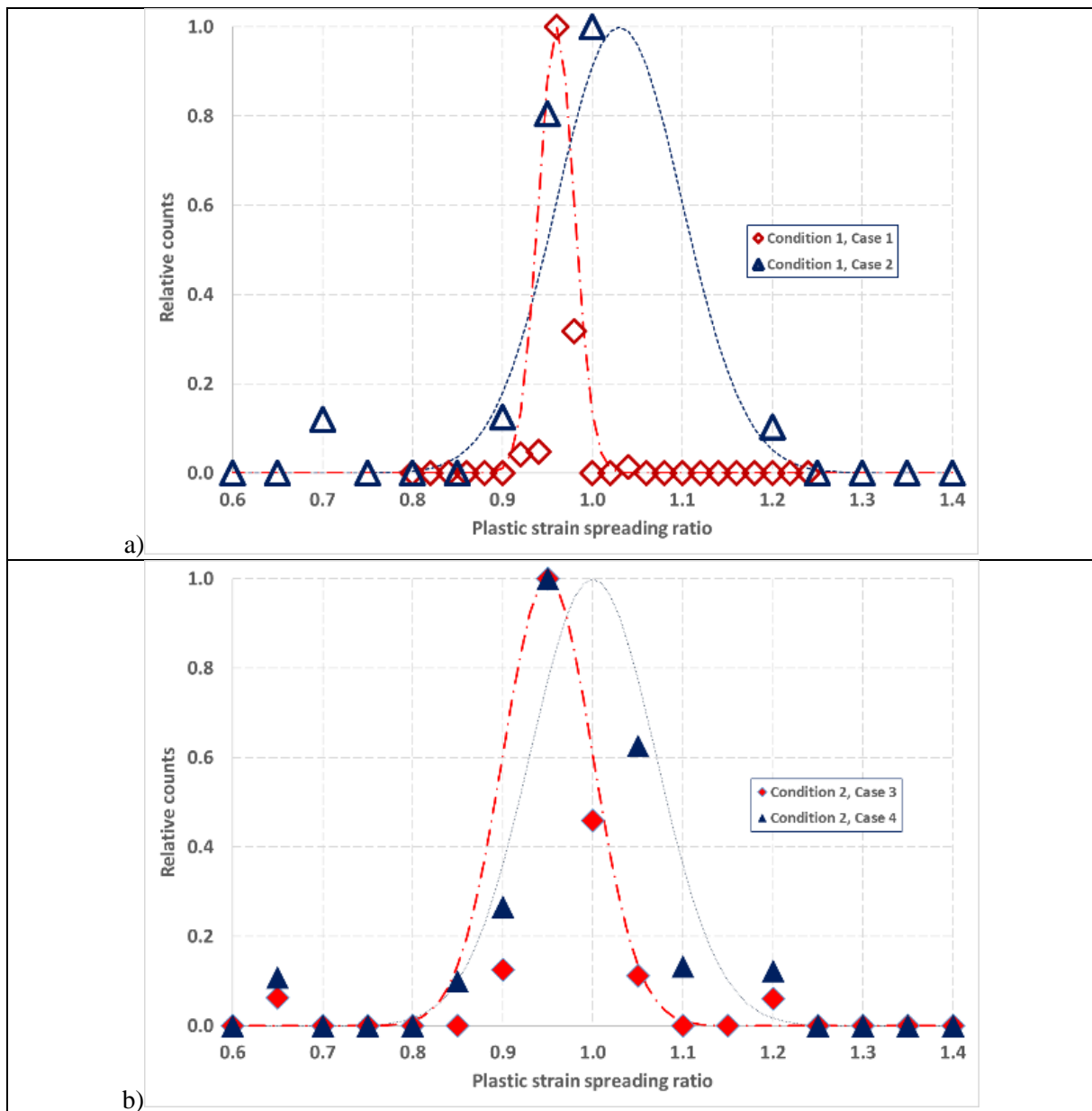


Figure 6

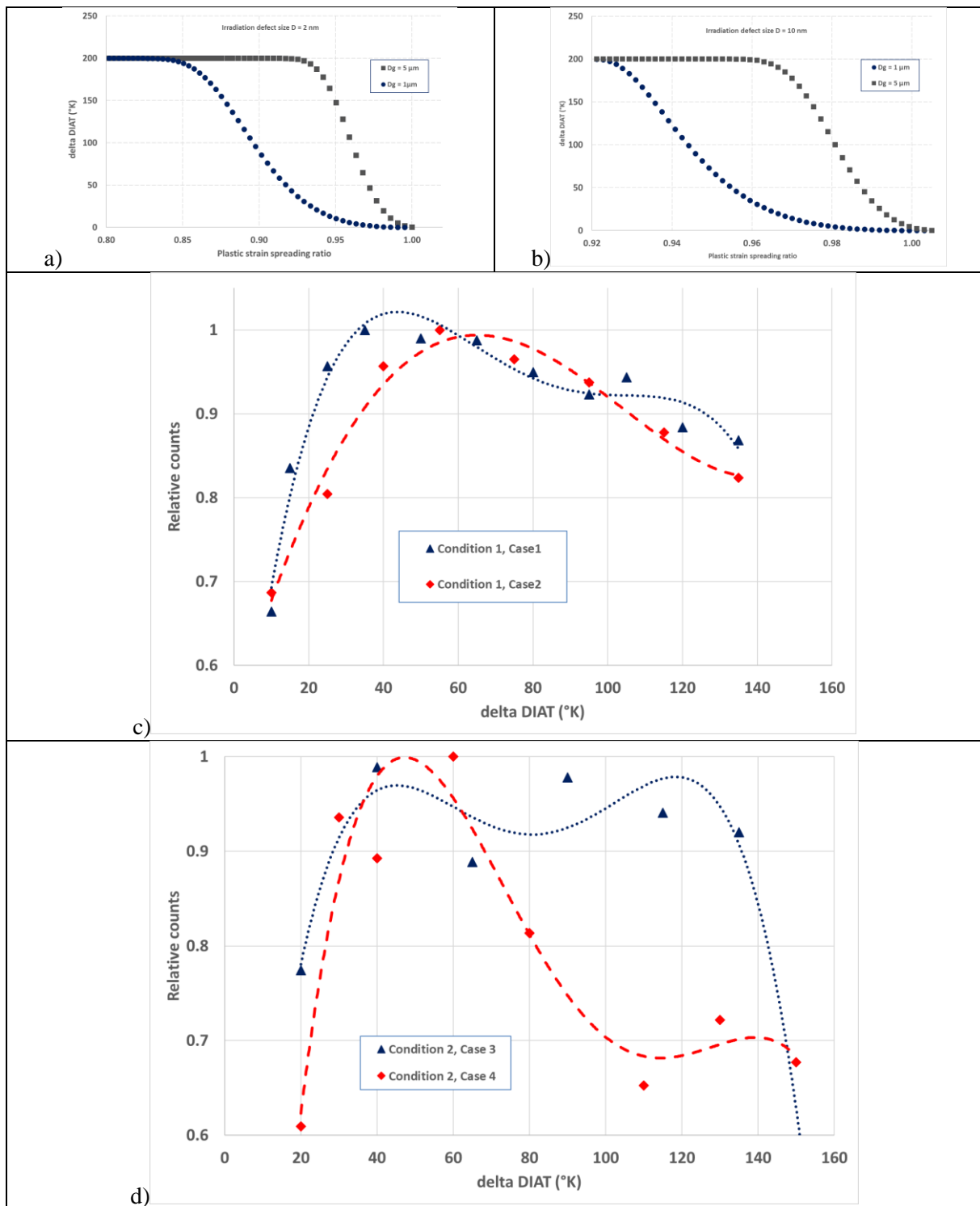


Figure 7

